Adiabatic Shear Band Modeling
in Inconel-718 Alloy

Stefano Dolci[1], Kelly Carney[1], Paul Du Bois[1] and Cing-Dao Kan[1]

1 Center for Collision Safety and Analysis, George Mason University, Fairfax, VA

Abstract

The failure mechanism for thick metal plates impacted by blunt projectiles is known as an adiabatic shear band (ASB), which results in a catastrophic failure due to concentrated shear deformation. ASB is generally considered to be a material or structural instability and as such is not controllable. ASBs are a thermodynamic phenomenon occurring at high strain rates and are characterized by large deformations, localized in a narrow band consisting of highly sheared material. Due to the extreme localization of the shear band it is difficult to model it using FEM, because the mesh size needed to capture it is often not practical for real applications.

ASBs can control failures in ballistic impacts. For example, the strength characteristics of Inconel 718 are superior to those of Titanium 6Al4V, in quasi-static conditions. Hence, the ballistic limit for the same geometry plates of these materials should be very different. Unexpectedly, tests show that the materials have a similar ballistic limit for a 0.5" plate. The explanation for this similarity is that, inside the ASB the temperature rises to above 700°C, where Inconel undergoes a phase transformation that makes it brittle, causing a sudden failure. Ti6Al4V HPC lattice has a different microstructure than Inconel's, and so its ASB behavior also differs.

2D analyses are presented, with progressively reduced element sizes until ASB appearance. ASBs of Inconel are shown to have a width of approximately 5 μm. This is far smaller than an element from an "industrial size" mesh. The elements of the mesh need to be smaller than the ASB width in order to capture the localization of shear and the consequent temperature rise in that region.

As adiabatic shear band modeling exhibits a strong dependency on mesh size, we propose to neutralize the effects of different mesh dimensions by implementing a new regularization algorithm. The new algorithm will increase the amount of plastic work converted into heat as function of mesh size, where ASBs will occur. The updated model will replicate the ASB characteristics obtained with the ultra-fine 2D mesh using an "industrial size" mesh.

Introduction

Inconel 718 has a Young's Modulus of 210 GPa, a yield stress at quasi-static rate at room temperature of 980 MPa and an ultimate stress in the same quasi-static condition of 1375 MPa41. Titanium 6Al 4V, under the same conditions has a Young's modulus of 113.8 GPa, a yield stress of 880 MPa and an ultimate stress of 950 MPa42. According to these numbers, the ballistic limit for same geometry plates of these materials should be very different. Inconel should overperform the ballistic limit of Titanium significantly. Unexpectedly, tests show that the materials have a similar ballistic limit for the 0.5 inches plate (Figure 1).
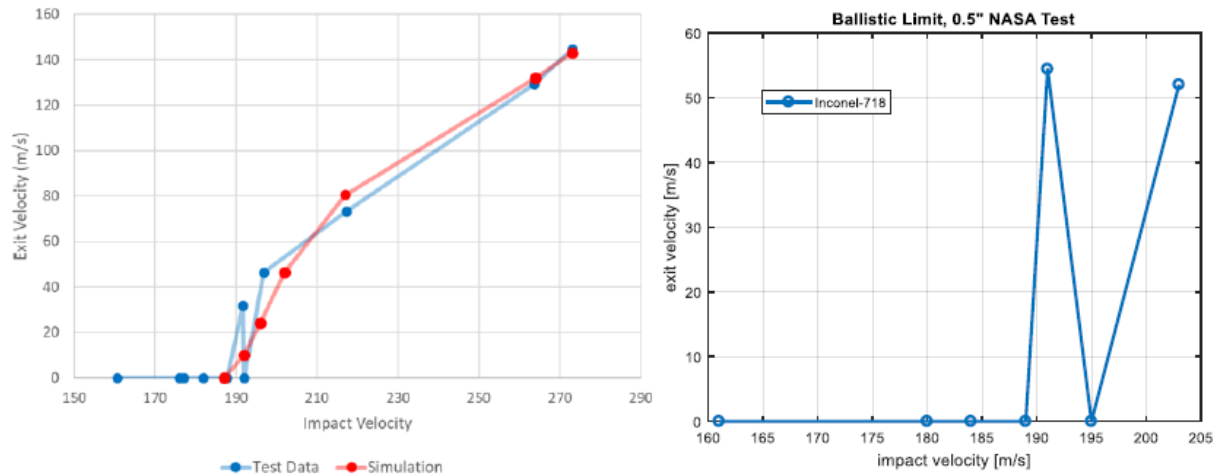
Figure 1: a) Titanium and b) Inconel 0.5' plates ballistic limits [1] [2]

Both materials under these conditions have a failure mode known as ASB. The similar results in the ballistic performances is most likely caused by the different microstructure of Inconel 718 in comparison to Ti6Al4V HPC lattice. Inconel at temperature above 700°C undergoes a phase transformation that makes it brittle[3]. Moreover, Inconel has a melting point of 1260°C[4] while Ti6Al4V has a melting point of 1604°C[5].The proposed explanation for this peculiar result is that inside the ASB the temperature raises to the point where Inconel becomes brittle causing a sudden failure. Unfortunately, the ASB of 0.5 inches Inconel plates has a width of approximately 5 μm, compared to Ti6Al4V that have an ASB width of approximately 50 μm. This is one of the reasons why the current material models are unable to simulate ballistic impact producing an ASB using a "industrial size mesh". The elements of the mesh need to be smaller than the ASB width in order to capture the localization of shear and the consequent temperature raise in that region. This would imply the usage of a mesh size smaller than 5 μm (for Inconel) which will lead to a model of many tenth of millions of elements and a prohibitive computational time. The proposed solution to this problem is to implement a regularization method that would allow (under the proper loading conditions, strain, strain rate, and temperature) the material failure with an ASB mechanism.

Adiabatic Shear Bands

Literature Review

Adiabatic shear bands represent thermo-viscoplastic instabilities and are often observed in ductile metals subjected to high rates of loading, because there is insufficient time to conduct away heat during the event. Such shear bands can be the dominant mode of failure in an impact event and are particularly common in impacts involving ductile metals subjected to overall compression and also in the perforation and punching of sheets and plates. Adiabatic shear bands are also observed in applications such as high-speed machining, where they limit the speed of the manufacturing process.[6]

Wright and Walter[7] pioneered the use of numerical simulation to follow the evolution of an adiabatic shear band. Feng and Bassim[8] assert that the growth of the ASB is affected by the strain hardening, thermal softening and thermal conduction. Using a rate-dependent equation they were able to simulate ASB initiated at local material defects in ANSYS. They described the modeling of the ASB as composed of 3 phases. In the first

stage, there is no plastic deformation. In the second stage, the strain hardening and thermal softening compete with each other. During the third stage, the thermal softening dominates.

Lee and Lin[9] investigated the plastic deformation behavior of titanium alloy (Ti–6Al–4V) at strain rate ranging from $5x10^2$ to $5x10^3$ s^{-1} in the temperature range between room temperature and 1100°C. They found that ASB are precursors to fracture and hardness and thickness of the adiabatic shear bands are found to change directly with the β-transus temperature. The increasing of temperature causes a decrease of the microhardness of the shear bands, while the thickness of the shear bands is found to increase with the temperature. The same authors in another paper[10] studying the high-temperature deformation behavior of Ti6Al4V alloy at constant strain rate of 2x103s-1 found that adiabatic shear bands are the sites where the fracture of the material occurs, and that the thickness and microhardness of adiabatic shear bands vary completely with temperature. It appears by their microstructural observations that the dislocation density decreases linearly with temperature. Moreover, the dislocation cell size increases with temperature, but decreases with dislocation density. The flow stress is related to the dislocation cell size by an inverse linear relationship.

Delorme[11] reports that the mechanism of softening and formation of adiabatic shear bands is still not well understood, but it is generally accepted that the process is related to a phenomenon known as dynamic recrystallization. Dynamic recrystallization refers to a rearrangement of the microstructure in a material undergoing high strain rate, high temperature deformation. This process is characterized by a refinement of grains and decrease in dislocation density and differs from static recrystallization in that the kinetics are much faster and the refined grains are very small. Materials undergoing dynamic recrystallization lose mechanical properties and soften during this process.

Dynamic recrystallization (DRX) was initially observed and proposed as a mechanism for ASB by Meyers and Pak[12] and has since been substantiated by the studies of De Andrade[13] and Hines and Vecchio[14]. DRX has been studied from a numerical perspective and has been applied to ASB formation by Chichili[15], Medyanik[16] and more recently by Dolinski[17]. The main observation that suggests the occurrence of dynamic recrystallization is that the ASB contains very fine grains with a comparatively low dislocation density. The formation of new grains by a static process has been ruled out by Hines and Vecchio[14] and calculations based on the time required for diffusion under static recrystallization conditions. The mechanism for the initiation of dynamic recrystallization is not yet fully understood. Initially, Meyers and Pak proposed a process of micro grain rotation and sliding or micro grain boundaries, Rittel[18] considers the mechanism as an athermal process brought on by buildup of strain energy due to cold work, as opposed to a thermally activated process as in the model of Medyanik. The main argument that Rittel makes for an athermal process is that high temperatures are not a prerequisite for the initiation of ASBs, since the severe temperature rise does not begin to occur until after localization has been initiated. Dynamic recrystallization has been shown to require a critical temperature to initiate by Medyanik, which depends on the applied strain rate. This temperature is shown to be approximately 0.4Tm at strain rates above 100/s. According to Landau et al.[19] the concurrent occurrence of different mechanisms including the emergence of dislocations, texture development, grain rotation and refinement results in the evolution of the microstructure within ASBs. They contest the leading opinion is that a competition between strain rate hardening and thermal softening that determines the onset of the failure. The authors also disagree that adiabatic shear is an instability and points out that contrary to the current paradigm, it was recently shown that instead of thermal softening mechanisms, microstructural softening transformations such as dynamic recrystallization (DRX) are responsible for adiabatic shear failure. Those transformations are dictated by the stored energy of cold work, so that energy considerations can be used to macroscopically model the failure mechanism.

Boakye-Yiadom[20] explained that because of the very narrow nature in the microstructure of the ASB (~1 to 350μm) and the rapid rates of deformation, it is virtually impossible to observe their evolution and mechanism

of formation during an impact. He explains the evolution in the microstructure of the ASB and concludes that for BCC ferritic-pearlitic hardenable steel, concurrent occurrence of emergence of dislocations, texture development, breaking of elongated grains, grain rotations and refinements result in the observed structure within ASBs in impacted specimens. It was also asserted that the occurrence of Dynamic Recovery (DR) and Dynamic Recrystallization (DRX) alone would not be sufficient to explain the observed microstructure within the evolved ASBs in impacted 4340 steel specimens because of the presence of refined and nano-grains with high density of dislocation. In this study, it was also observed that the initiation of ASBs in AISI 4340 steel during impact occurs when the microstructure is highly inhomogeneous. Specimens tempered at lower temperatures are more susceptible to the formation of ASBs because of the higher inhomogeneities.

There has been relatively little research on the shear band evolution of Inconel 718. Song et al.[21] studied the effects of different heat treatments on the dynamic shear response and the adiabatic shear localization characteristic of Inconel 718 alloy and estimated a shear band width of about 10μm by the SEM micrograph for aged Inconel tested at a strain rate of $8x10^5$ s^{-1}. The results indicate that the aged Inconel 718 with higher yield strength and lower strain hardening rate is easier to form an adiabatic shear band (ASB) than that of the solution treated Inconel 718 under dynamic shear loadings.
Pereira and Lerch[22] showed that during blunt object impact, typically exemplified by containment situations of blade-out events in jet engines, annealed Inconel 718 material could absorb a significantly larger amount of energy compared to its precipitation strengthened counterpart during blunt object impact. DeMange et al.[23] presented similar results in a combination of high strain rate (10^3 s^{-1}) compression tests and top hat shear tests. This result could indicate that high elongation and better strain hardening capabilities reduced the tendency for adiabatic shear localization and the resulting more wide-spread deformation.

Recently, detailed investigations of the microstructure within shear bands formed in Inconel 718 during machining and controlled dynamic shear-compression deformation were conducted by Johansson et al.[24]. The top-hat tests showed a very narrow 4–5 μm wide shear localized bands with recrystallized grains down to the order of 20–300 μm and a very narrow transition zone to adjacent material.

Regarding Inconel 718 ASB FEM simulations, most of the publications are focused on the simulation of machining e.g. Lorentzon et al.[25], Jafarian et al.[26]. Erice et al.[27] studied the ASB generated by a blunt object in impact simulations. In general, the simulations are able to capture the essential features of shear localization. However, Ozel et al.[28], comparing experimental results of machining of Inconel 718 with 3D FEM simulations, emphasized the role of the material model, when applied to large strain and high temperature changes cases, as well the importance of using appropriate meshing. In the study by DeMange et al.[23], numerical simulations of Inconel 718 top-hat specimens during dynamic testing were performed. Simulations of the shear band formation showed very high strain rates and temperatures, with higher values reached in the aged condition compared to the annealed. However, the constitutive model was not calibrated against high-strain-rate tests at elevated temperature. Moreover, the load–displacement curves from the simulations and experiments of the top-hat tests were not compared, therefore the agreement with experiments remains unclear. Johansson et al.[29] Studied the effects of microstructure on the strain localization behavior during dynamic shear deformation of Inconel 718 by experiments and numerical simulations of Split-Hopkinson tests of specimens with top-hat geometry. The results show that strain localization is promoted by small grain size and precipitation hardening, whereas large grains and solution annealing largely suppressed the formation of shear bands. In addition, a smaller fillet radius facilitated the initiation of shear bands. Finite element simulations were able to reproduce the most important features of both global load displacement histories, and presence of shear localization. Simulations of the local deformation during localization showed that temperatures exceeding 750 °C (locally above 1000°C) and strain rates in the order of $2x10^5$ s^{-1} were reached in the band.
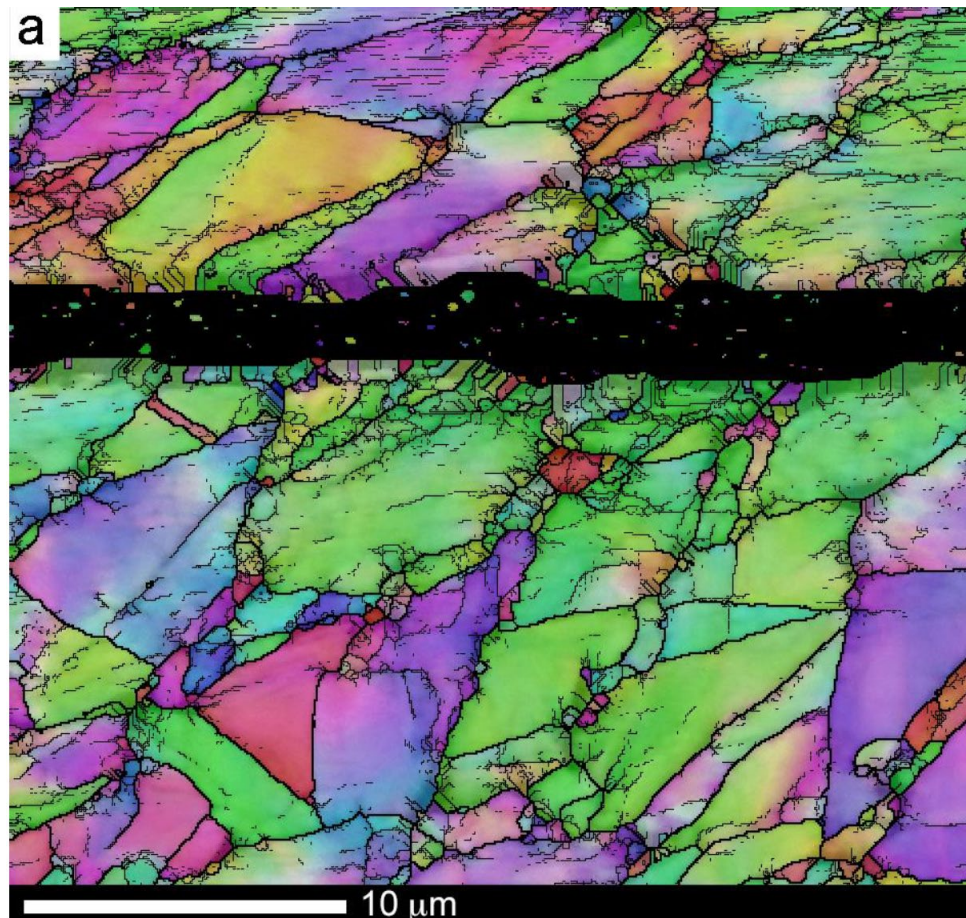
Figure 2: Inconel 718 EBSD map (superimposed on the band contrast) of the region adjacent to the shear[24]

Erice et al.[27] performed a performed a numerical and experimental study of ballistic impacts at various temperatures on Inconel 718 superalloy plates using a coupled elasto-plastic damage constitutive model with lode angle dependent failure. The numerical study showed that the mesh size is crucial to predict correctly the shear bands detected in the tested plates. Many approaches have been proposed in the literature to overcome the mesh sensitivity of finite element solutions but very few about the specific issues of ASB.

Almasri [30] speculates that a nonlocal gradient method associated with a dynamic length scale could be applied to regularize the FEM results and noticed that the kinetic energy and strain energy stored in the body are both related linearly to the shear band length, while viscous dissipation is not. Teng[31] noticed that one of the simplest ways to remedy mesh size sensitivity is to equip the element size with a physical meaning. This idea can be directly implemented without any modification of commonly used material constitutive models and fracture models. Redanz[32] suggested that the mesh size could be approximately equal to the particle size. Alternatively, the mesh size can be associated with the size of a fracture process zone ahead of a propagating crack, where micro-cracks or micro-voids nucleate, grow, and eventually coalesce with the major crack. The third type of approach is the development of nonlocal constitutive models, in which a characteristic or internal length scale is implemented. In such a way, the prediction of fracture is not only controlled by stresses and strains but also related to material microstructures.

Several formulations originated from this idea have been proposed, e.g. Tvergaard and Needleman[33]. The characteristic length was considered to represent the average grain size or the average void spacing. However, these approaches are not applicable to the failure analysis of large structures such as aircrafts or car collision,

due to limitation of computational resources. Teng identified high strain gradient and strain softening as two critical factors leading to mesh size sensitivity. He found that crack growth and residual velocities at high impact velocities are not dependent on element size. However, the prediction of ballistic limit and the evolution of adiabatic shear bands is sensitive to the mesh size[31]

It's evident from the literature review that two elements are crucial in correctly predicting the ASB developing process: the correct stress flow at high strain rates and the mesh density. It appears that no successful attempt to regularize failure for mesh size, suitable for large analysis, to simulate ASB has been reported.

Mesh sensitivity to ASBs 2D Study

A series of 2D simulations have been performed with in LS-DYNA® to verify the capability of the isotropic elasto-thermo-visco-plastic constitutive relationship implemented in *MAT_224 to simulate ASBs. The use of 2D elements allows a much smaller mesh size than a full 3D structural representation. The underlying physics and dimensions of the ASB can therefore be investigated in the 2D study. 2D shell element formulation 13, which uses plane strain solid elements to represent a cross-section of a structure were used. The geometry of the simulated structure is visible in Figure 3 and is the same for each simulation having varying overall dimensions, element dimensions and boundary conditions. The simulation is not of an actual structure, but is idealized in order to readily create ASBs, using a relatively small number of elements. A list of the simulations performed is shown in Table 1.

2D SHEARBAND ANALYSIS -

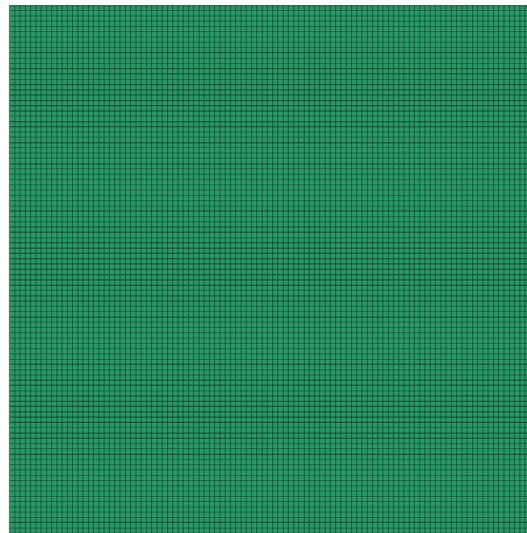**Figure 3: 2D simulations geometry**

Table 1: 2D Simulations

Simulation Name	# of Elements	Elements Size [μm]	Boundary Conditions	Overall Edge Size [μm]
Inco_100x100_LC1_BC1_05	10000	0.5	1	50
Inco_100x100_LC1_BC1_1	10000	1	1	100
Inco_100x100_LC1_BC1_4	10000	4	1	400
Inco_100x100_LC1_BC1_20	10000	20	1	2000
Inco_100x100_LC1_BC1_200	10000	200	1	20000
Inco_100x100_LC1_BC8_05	10000	0.5	8	50
Inco_100x100_LC1_BC8_1	10000	1	8	100
Inco_100x100_LC1_BC8_4	10000	4	8	400
Inco_100x100_LC1_BC8_20	10000	20	8	2000
Inco_100_4_LC1_BC1	225	4	1	100
Inco_100_4_LC1_BC8	225	4	8	100
Inco_100_10_LC1_BC1	100	10	1	100
Inco_100_10_LC1_BC8	100	10	8	100

Boundary Conditions

The simulations were performed with 2 sets of boundary conditions; visible in Figure 4. In both sets, the nodes marked with the red were constrained in all directions while a loading curve with velocity in y direction was applied to the nodes marked in blue. The boundary conditions were varied to determine which set provided a better match to physical ASB conditions.
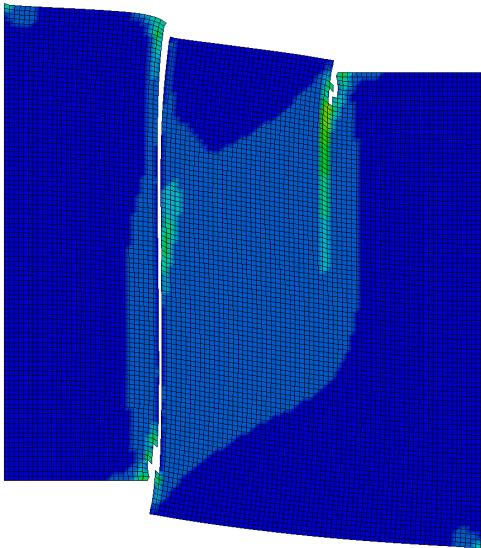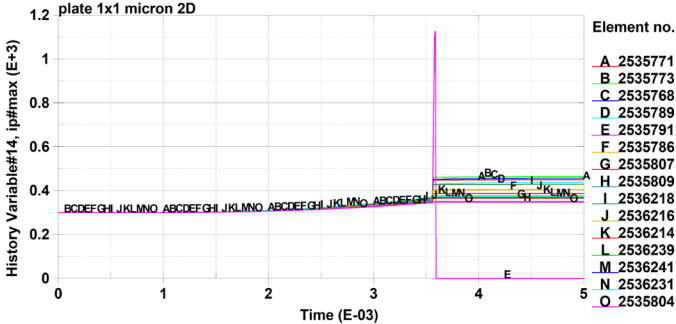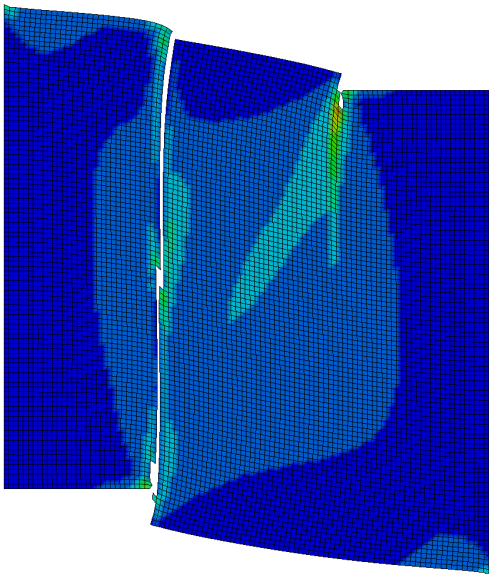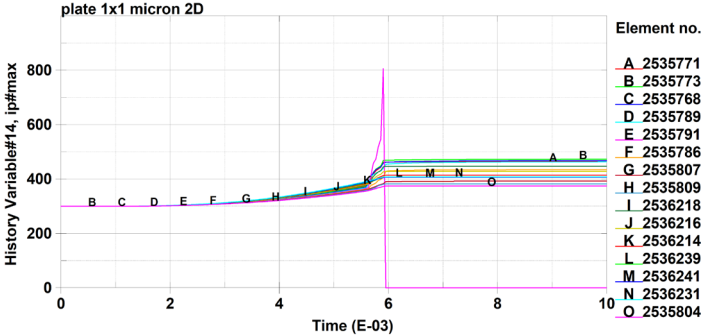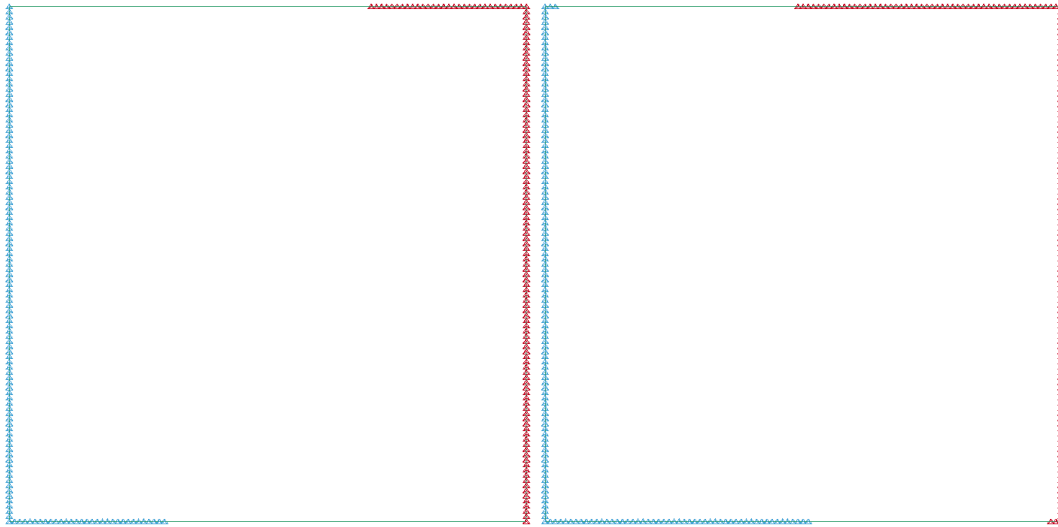

**Figure 4: Boundary conditions a) 1 and b) 2**

Simulation Results

The simulation results are reported in Table 2. It is important to note that the raise of temperature is more localized across the shear band in the models with the smaller element size. When the element size chosen is not small enough, the model is not able to simulate the failure with a shear band mode, let alone produce an adiabatic shear band. For a shear band to be adiabatic, it must show a decisive increment of temperature across the band direction; only in one element in a very short time. To be physical, the velocity of propagation of the band must also be extremely high.
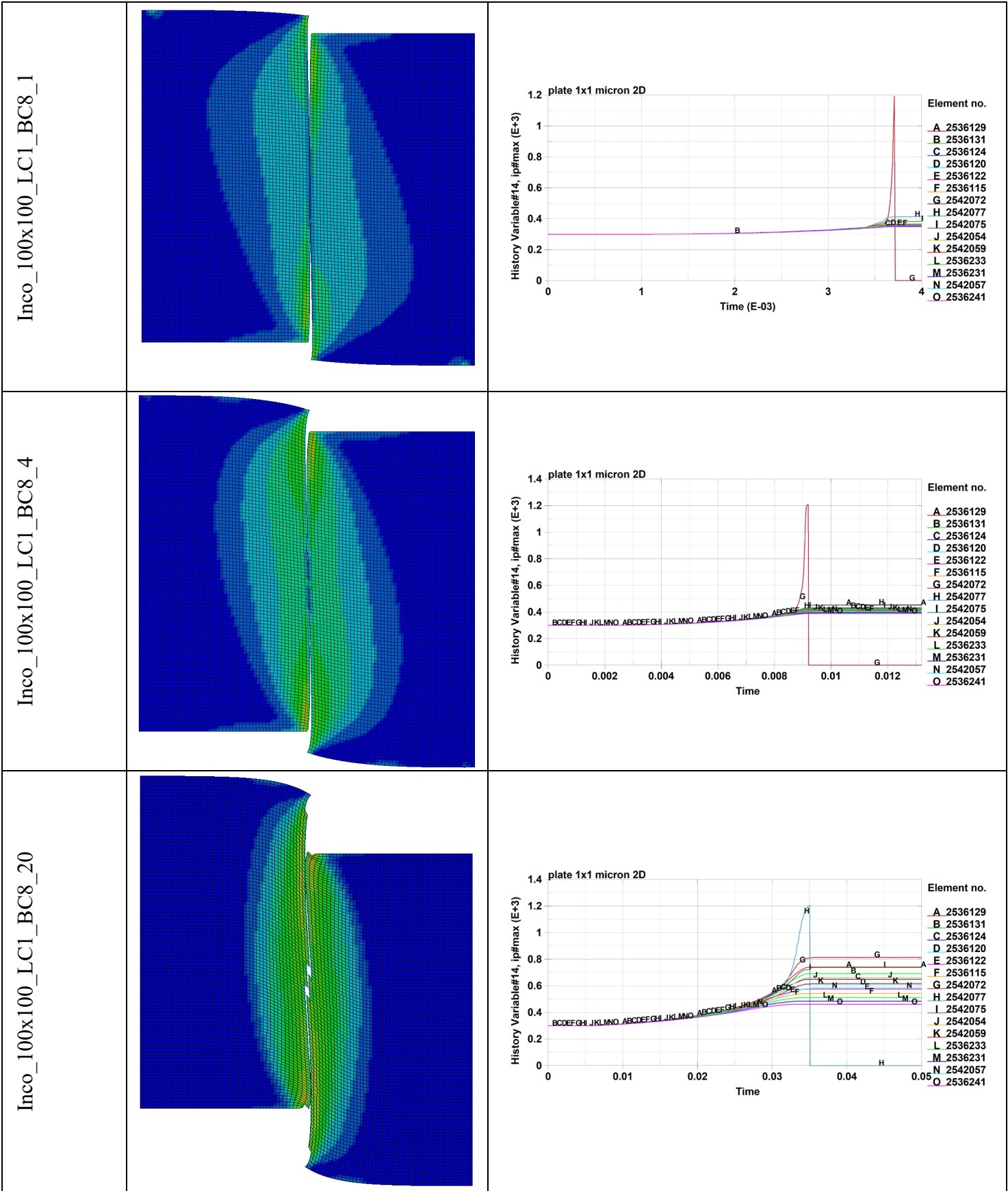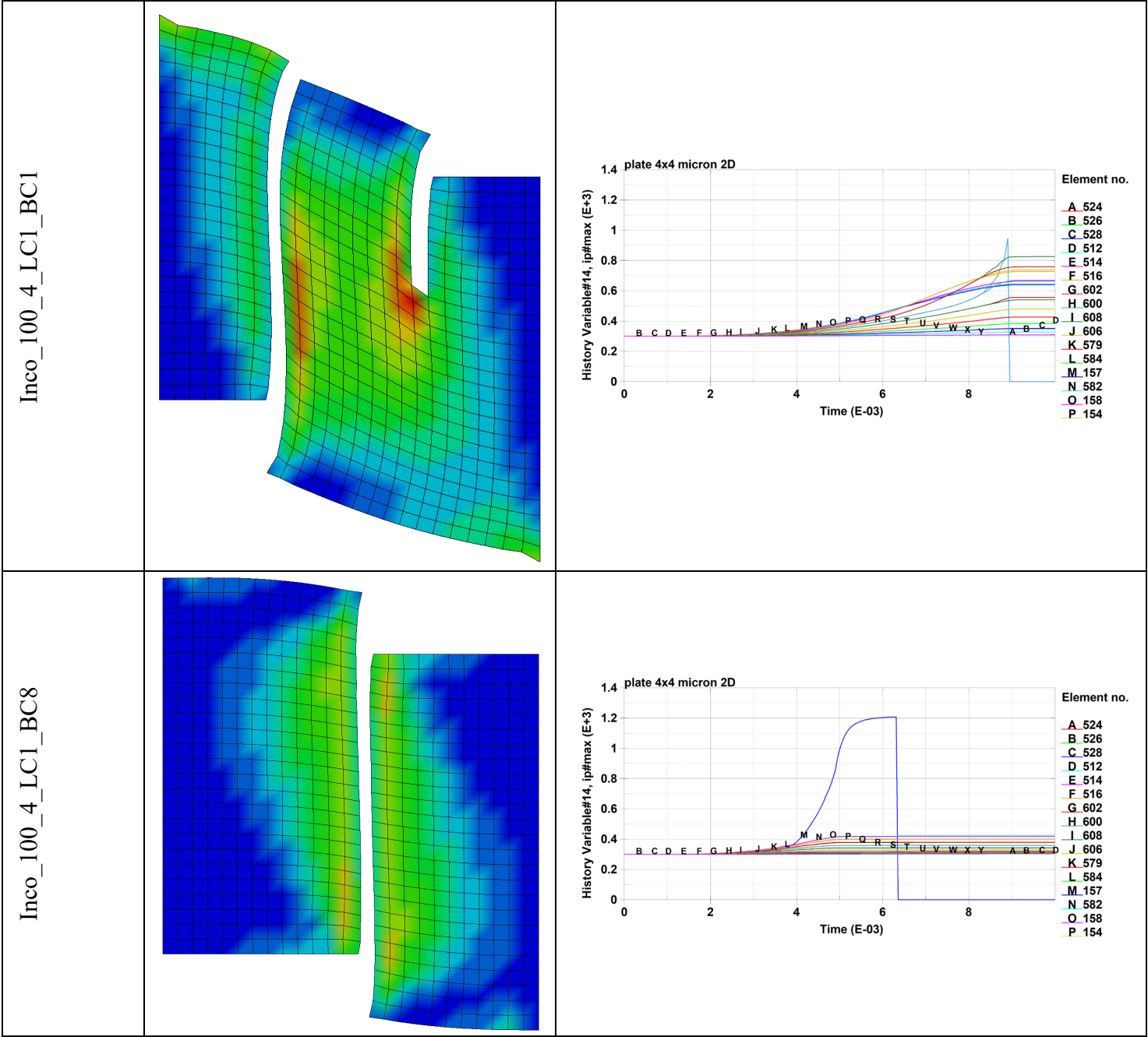
Table 2: Simulation Results

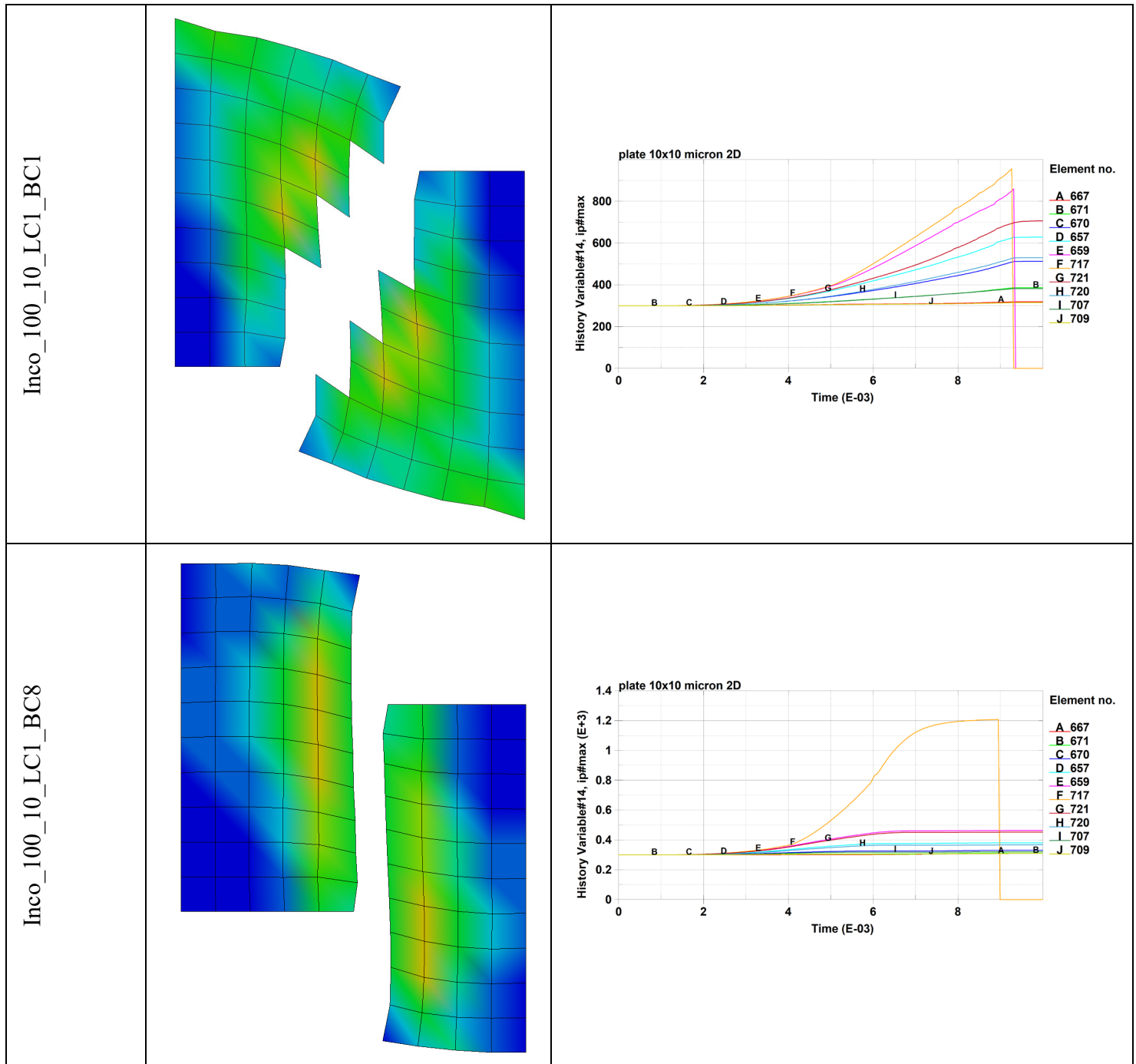| Simulation Name	Effective Plastic Strain Contours	Temperature Shear Band Elements
Inco_100x100_LC1_BC1_05		
Inco_100x100_LC1_BC1_1		
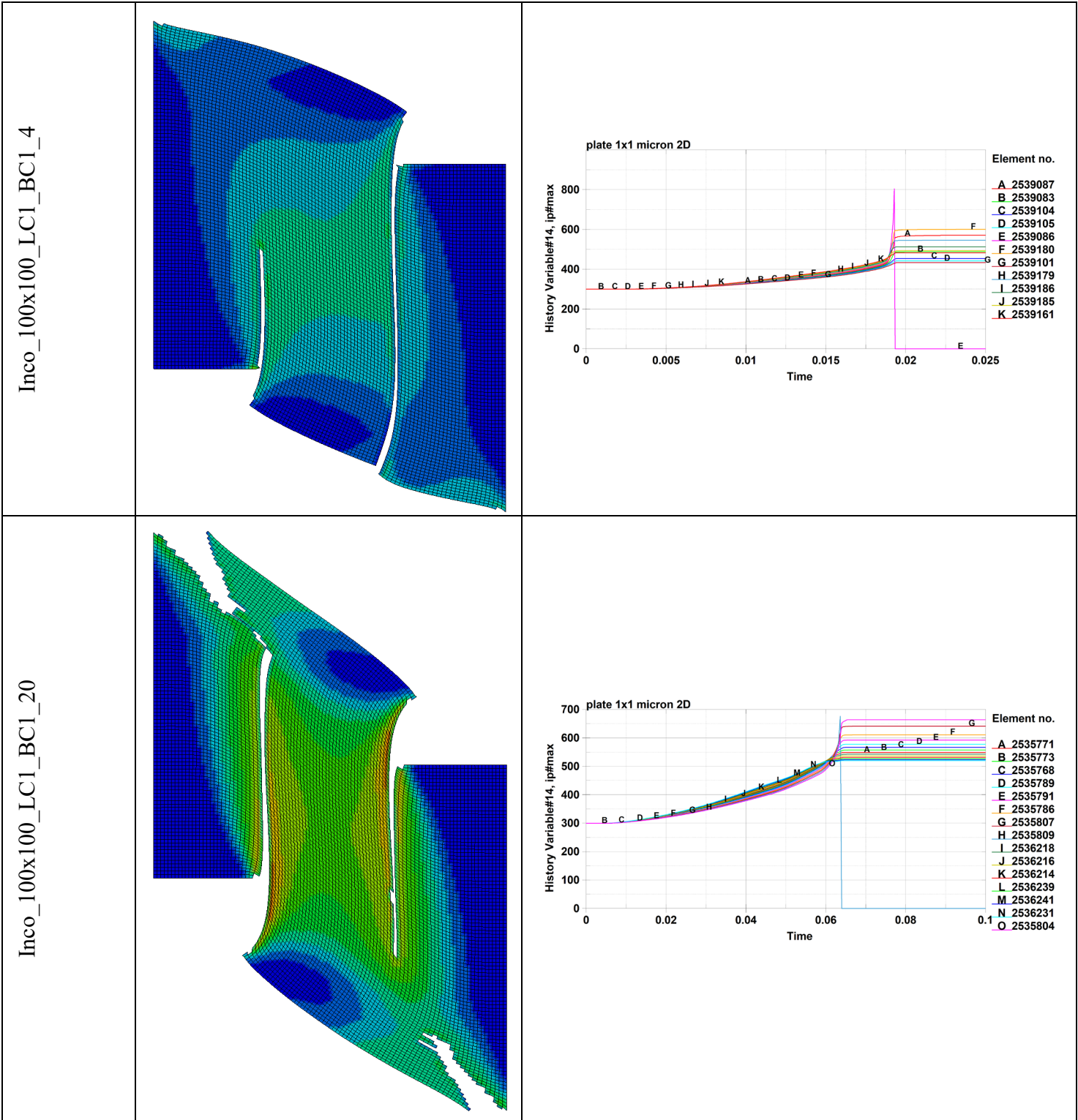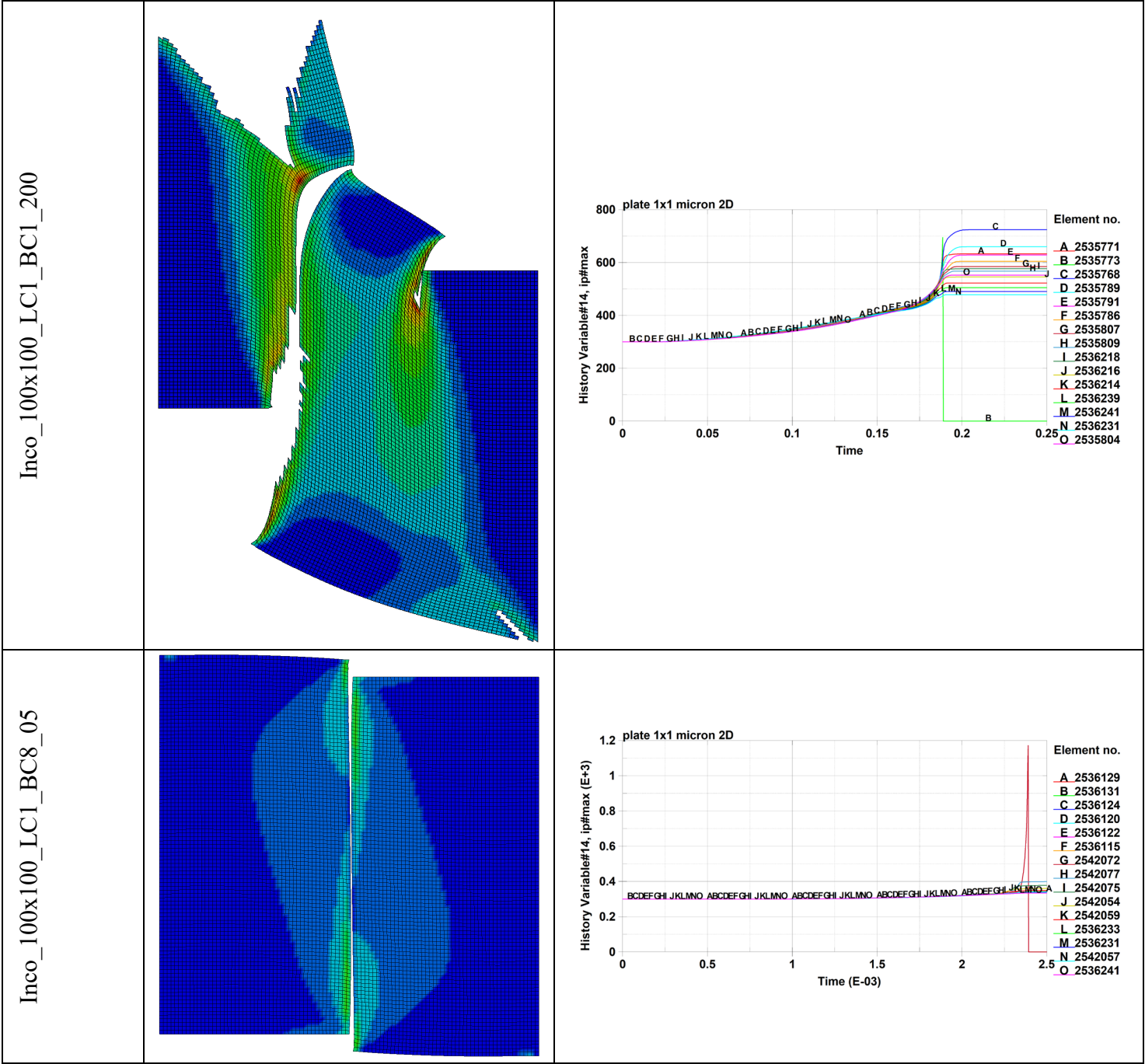
For the first set of boundary conditions mesh sizes smaller than 4 μm can predict a clear ASB with a width of 1 element. The 4 μm mesh size is still able to give a good prediction but the shear band temperature increase is not as localized as in the smaller elements simulations.

For the second set of boundary conditions mesh sizes smaller or equal than 4 μm can predict a clear ASB with a width of 1 element. The 20 μm mesh size is still able to give a good prediction but the shear band temperature increase is not as localized as in the smaller elements simulations.

The brittle temperature of Inconel happens at around 973K, this temperature is reached in all the analysis with a mesh size below 4 μm for the first set of boundary condition and for all the analysis with the second set of

boundary condition. The curves in some of the graphs are not reaching the actual maximum temperature due to insufficient sampling frequency.

The shear band propagation rate calculated for Inconel is approximately 680 to 6500 ms^{-1} (see Table 3) for the smaller element mesh size with a temperature in the shear band reaching over 1100K. The results are consistent with similar tests reported in literature[34]. It appears evident that the failure mechanism for Inconel for larger element size is not ASB, therefore, only a sufficiently dense mesh is capable at the current state of capturing the phenomena.

It is interesting to note that strictly for mesh-size only regularization, as currently implemented in *MAT_224 was not required to produce ASBs in this study. Given that necking-like localization is not significant in an ASB, this is not surprising.

Table 3: Crack Propagation Velocity

Simulation Name	Crack Propagation Velocity[m/s]
Inco_100x100_LC1_BC1_05	678
Inco_100x100_LC1_BC1_1	267
Inco_100x100_LC1_BC1_4	97
Inco_100x100_LC1_BC1_20	90
Inco_100x100_LC1_BC1_200	N/A
Inco_100x100_LC1_BC8_05	6464
Inco_100x100_LC1_BC8_1	3267
Inco_100x100_LC1_BC8_4	1839
Inco_100x100_LC1_BC8_20	224
Inco_100_4_LC1_BC1	113
Inco_100_4_LC1_BC8	352
Inco_100_10_LC1_BC1	N/A
Inco_100_10_LC1_BC8	30

It is significant that with no changes to the material model, once elements were 4 μm or smaller, adiabatic shear bands appeared. The physics of these simulations appear to match the conditions which are described in the literature. Unfortunately, the mesh size needed to predict adiabatic shear bands are too small to be of any practical use in actual applications. This confirms the need of a new type of regularization, which can lead to the physical failing mechanism for any mesh size.

Conclusions

As expected, the ASB can be simulated by LS-DYNA *MAT_224 if the element mesh size is small enough. This confirms the hypothesis that element mesh and characterization of the material strain rate sensitivity are crucial to correctly simulate the ASB phenomenon. The width of the ASB in Inconel 718 was shown to be approximately 1 μm. This very small width, and the resulting required mesh size, strengthens the need of implementing new methods to obtain a correct stress flow characterization, and to develop a mesh size regularization that will adjust the amount of plastic work converted into heat in order to capture the right physical behavior of the ASB.

Acknowledgments

References

[1] S. Haight, L. Wang, P. Du Bois, K. S. Carney, and C.-D. Kan, "Development of a Titanium Alloy Ti-6Al-4V Material Model Used in LS-DYNA." May 26, 2015.

[2] S. Dolci, K. S. Carney, L. Wang, P. Du Bois, and C.-D. Kan, "The effect of Inconel-718 high strain rate sensitivity on ballistic impact response using *MAT_224," presented at the 16th International LS-DYNA Users Conference, 2018, p. 16.

[3] M. Jambor, O. Bokůvka, F. Nový, L. Trško, and J. Belan, "Phase transformations in nickel base superalloy INCONEL 718 during cyclic loading at high temperature," *Prod. Eng. Arch.*, vol. 15, pp. 15–18, Jun. 2017, doi: 10.30657/pea.2017.15.04.

[4] MatWeb, "Special Metals INCONEL® Alloy 718." http://www.matweb.com/search/DataSheet.aspx?MatGUID=94950a2d209040a09b89952d45086134&ckck=1 (accessed Nov. 07, 2018).

[5] MatWeb, "Titanium Ti-6Al-4V (Grade 5), Annealed." http://www.matweb.com/search/datasheet.aspx?MatGUID=a0655d261898456b958e5f825ae85390 (accessed Nov. 07, 2018).

[6] K. T. Ramesh, "High Strain Rate Part D 33. High Strain Rate and Impact Experiments," p. 31.

[7] T. W. Wright and J. W. Walter, "On Stress Collapse in Adiabatic Shear Bands.," p. 46.

[8] H. Feng and M. N. Bassim, "Finite element modeling of the formation of adiabatic shear bands in AISI 4340 steel," *Mater. Sci. Eng. A*, vol. 266, no. 1, pp. 255–260, Jun. 1999, doi: 10.1016/S0921-5093(99)00026-X.

[9] W.-S. Lee and C.-F. Lin, "Plastic deformation and fracture behaviour of Ti–6Al–4V alloy loaded with high strain rate under various temperatures," *Mater. Sci. Eng. A*, vol. 241, no. 1, pp. 48–59, Jan. 1998, doi: 10.1016/S0921-5093(97)00471-1.

[10] W.-S. Lee and C.-F. Lin, "High-temperature deformation behaviour of Ti6Al4V alloy evaluated by high strain-rate compression tests," *J. Mater. Process. Technol.*, vol. 75, no. 1, pp. 127–136, Mar. 1998, doi: 10.1016/S0924-0136(97)00302-6.

[11] J. Delorme, "Extension of a finite element model to 2D for the prediction of adiabatic shear bands," Sep. 2012, Accessed: Sep. 18, 2018. [Online]. Available: https://mspace.lib.umanitoba.ca/xmlui/handle/1993/8916.

[12] M. Meyers and H.-R. Pak, "Observation_of_an_adiabatic_shear_band_i20160422-29854-16ih0oh.pdf." https://s3.amazonaws.com/academia.edu.documents/44996847/Observation_of_an_adiabatic_shear_band_i20160422-29854-16ih0oh.pdf?AWSAccessKeyId=AKIAIWOWYYGZ2Y53UL3A&Expires=1551393628&Signature=qeojPmbzd4AkEOWyf5giii05XXc%3D&response-content-disposition=inline%3B%20filename%3DObservation_of_an_adiabatic_shear_band_i.pdf (accessed Feb. 28, 2019).

[13] U. De Andrade, M. Meyers, A. Chokshi, and K. Vecchio, "Dynamic recrystallization and grain size effects in shock hardened copper," *J. Phys. IV Colloq.*, vol. 04, no. C8, pp. C8-361-C8-366, 1994, doi: 10.1051/jp4:1994855.

[14] J. A. Hines and K. S. Vecchio, "Recrystallization kinetics within adiabatic shear bands," *Acta Mater.*, vol. 45, no. 2, pp. 635–649, Feb. 1997, doi: 10.1016/S1359-6454(96)00193-0.

[15] D. R. Chichili, K. T. Ramesh, and K. J. Hemker, "Adiabatic shear localization in α-titanium: experiments, modeling and microstructural evolution," *J. Mech. Phys. Solids*, vol. 52, no. 8, pp. 1889–1909, Aug. 2004, doi: 10.1016/j.jmps.2004.02.013.

[16] S. Medyanik, W. Liu, and S. Li, "On criteria for dynamic adiabatic shear band propagation," *J. Mech. Phys. Solids*, vol. 55, no. 7, pp. 1439–1461, Jul. 2007, doi: 10.1016/j.jmps.2006.12.006.

[17] M. Dolinski, D. Rittel, and A. Dorogoy, "Modeling adiabatic shear failure from energy considerations," *J. Mech. Phys. Solids*, vol. 58, no. 11, pp. 1759–1775, Nov. 2010, doi: 10.1016/j.jmps.2010.08.007.

[18] D. Rittel, "A different viewpoint on adiabatic shear localization," *J. Phys. Appl. Phys.*, vol. 42, no. 21, p. 214009, Nov. 2009, doi: 10.1088/0022-3727/42/21/214009.

[19] P. Landau, S. Osovski, A. Venkert, V. Gärtnerová, and D. Rittel, "The genesis of adiabatic shear bands," *Sci. Rep.*, vol. 6, no. 1, Dec. 2016, doi: 10.1038/srep37226.

[20] S. Boakye-Yiadom, "Microstructural evolution of adiabatic shear bands in steel by impact," 2014, Accessed: Sep. 18, 2018. [Online]. Available: https://mspace.lib.umanitoba.ca/xmlui/handle/1993/24095.

[21] W. Song, M. Hu, H. Zhang, and Y. Jin, "Effects of different heat treatments on the dynamic shear response and shear localization in Inconel 718 alloy | Elsevier Enhanced Reader." https://reader.elsevier.com/reader/sd/pii/S0921509318305070?token=1B20F65DB474A87503BCCD9A9674329D8BEB3E2BC05C19315F068F2B8875BB3094A3DE56F402F5B15832A6E248B72C7C (accessed Mar. 14, 2019).

[22] J. M. Pereira and B. A. Lerch, "Effects of heat treatment on the ballistic impact properties of Inconel 718 for jet engine fan containment applications," *Int. J. Impact Eng.*, vol. 25, no. 8, pp. 715–733, Sep. 2001, doi: 10.1016/S0734-743X(01)00018-5.

[23] J. J. DeMange, V. Prakash, and J. M. Pereira, "Effects of material microstructure on blunt projectile penetration of a nickel-based super alloy," *Int. J. Impact Eng.*, vol. 36, no. 8, pp. 1027–1043, Aug. 2009, doi: 10.1016/j.ijimpeng.2009.01.007.

[24] J. Johansson, C. Persson, H. Lai, and M. Hörnqvist Colliander, "Microstructural examination of shear localisation during high strain rate deformation of Alloy 718," *Mater. Sci. Eng. A*, vol. 662, pp. 363–372, Apr. 2016, doi: 10.1016/j.msea.2016.03.080.

[25] J. Lorentzon, N. Järvstråt, and B. L. Josefson, "Modelling chip formation of alloy 718," *J. Mater. Process. Technol.*, vol. 209, no. 10, pp. 4645–4653, Jun. 2009, doi: 10.1016/j.jmatprotec.2008.11.029.

[26] F. Jafarian, M. Imaz Ciaran, D. Umbrello, P. J. Arrazola, L. Filice, and H. Amirabadi, "Finite element simulation of machining Inconel 718 alloy including microstructure changes," *Int. J. Mech. Sci.*, vol. 88, pp. 110–121, Nov. 2014, doi: 10.1016/j.ijmecsci.2014.08.007.

[27] B. Erice and F. Gálvez, "A coupled elastoplastic-damage constitutive model with Lode angle dependent failure criterion," *Int. J. Solids Struct.*, vol. 51, no. 1, pp. 93–110, Jan. 2014, doi: 10.1016/j.ijsolstr.2013.09.015.

[28] T. Ozel, I. Llanos, J. Soriano, and P.-J. Arrazola, "3d Finite Element Modelling of Chip Formation Process for Machining Inconel 718: Comparison of Fe Software Predictions," *Mach. Sci. Technol.*, vol. 15, no. 1, pp. 21–46, Apr. 2011, doi: 10.1080/10910344.2011.557950.

[29] J. Johansson, C. Persson, G. Testa, A. Ruggiero, N. Bonora, and Colliander, "Effect of microstructure on dynamic shear localisation in Alloy 718 | Elsevier Enhanced Reader." https://reader.elsevier.com/reader/sd/pii/S0167663616303854?token=D8B498690542F345A47DE82D6FF2D1CCDFC2E5B0D5 F9C46D21B834EA370F2559A7E31825F732AE9AAA4EBC48A944D4C4 (accessed Mar. 14, 2019).

[30] A. Almasri, "Dynamic Shear Bands in Metals under High Strain Rates," *LSU Dr. Diss.*, Jan. 2008, [Online]. Available: https://digitalcommons.lsu.edu/gradschool_dissertations/197.

[31] X. Teng, "High Velocity Impact Fracture," p. 330.

[32] P. Redanz, N. A. Fleck, and R. M. McMEEKING, "Failure of a Porous Solid from a Deep Notch," p. 17.

[33] V. Tvergaard and A. Needleman, "Effects of nonlocal damage in porous plastic solids," *Int. J. Solids Struct.*, vol. 32, no. 8–9, pp. 1063–1077, Apr. 1995, doi: 10.1016/0020-7683(94)00185-Y.

[34] M. Zhou, A. J. Rosakis, and G. Ravichandran, "Dynamically propagating shear bands in impact-loaded prenotched plates—I. Experimental investigations of temperature signatures and propagation speed," *J. Mech. Phys. Solids*, vol. 44, no. 6, pp. 981–1006, Jun. 1996, doi: 10.1016/0022-5096(96)00003-8.